In-plane optical features of the underdoped La_2CuO_4 based compounds: Theoretical multiband analysis

Ivan Kupčić*
Department of Physics, Faculty of Science, POB 331, HR-10 002 Zagreb, Croatia

The three-component *ab*-plane optical conductivity of the high-T_c cuprates is derived using the gauge invariant response theory, and compared to the data previously obtained from the optical reflectivity measurements in the La_2CuO_4 based families. The valence electrons are described by the Emery three-band model with the antiferromagnetic correlations represented by an effective single-particle potential. In the $0 < \delta < 0.3$ doping range, it is shown that the total spectral weight of the three-band model is shared between the intra- and interband channels nearly in equal proportions. At optimum doping, the low-frequency conductivity has a (non-Drude) nearly single-component form, which transforms with decreasing doping into a two-component structure. The mid-infrared spectral weight is found to be extremely sensitive to the symmetry of the effective single-particle potential, as well as to the doping level. The gauge invariant form of the static and elastic Raman vertices is determined, allowing explicit verification of the effective mass theorem and the related conductivity sum rules.

PACS numbers: 74.25.Gz 74.25.Nf
Keywords: superconductivity, high-T_c cuprates, $La_{2-x}Sr_xCuO_4$, optical properties, conductivity sum rules, Raman vertex functions

I. INTRODUCTION

Following the marginal Fermi liquid theory [1], the nested Fermi liquid theory [2] or the ordinary memory-function approach [3], the low-frequency excitations of the electronic system involved in the optical conductivity and electronic Raman scattering spectra of the overdoped high-T_c cuprates are described in terms of the frequency-dependent effective mass $m(\omega)$ and the frequency-dependent relaxation time $\tau(\omega)$, with a minor role played by selection rules or by normal-state coherence factors. Attempts to explain the measurements in the underdoped cuprates using similar single-component models have been unsuccessful. Anomalous low-frequency structures related to the superconducting (SC) pseudogap, the antiferromagnetic (AF) pseudogap, the two-magnon excitations or the density waves are observed in the latter crystals, usually in one or two (of four) "optical" channels (optical conductivity and A_{1g}, B_{1g} and B_{2g} Raman symmetries). [3, 4, 5, 6, 7, 8, 9, 10] Any theory of the low-frequency excitations in the underdoped cuprates should explain anomalies in both optical conductivity and Raman scattering spectra, taking the normal-state coherence effects properly into account.

The previous theoretical work on the optical conductivity of the underdoped cuprates [11, 12, 13, 14, 15, 16] is carried out for the one-band models with a particular care devoted to the treatment of strong local correlations responsible for the AF structure in the low-frequency conductivity, but no attention was paid to the (interband) optical processes in the visible part of the spectra. The principal physical problem is that when such one-band models are applied to the Raman spectra, then the resonant nature of the Raman scattering processes is ignored, because the intermediate states in the Raman scattering processes are treated in the static approximation. [17, 18] The first experimental evidence for the crucial role of the interband processes at $\hbar\omega \approx 1.75 - 2.75$ eV for the low-frequency physics of the high-T_c cuprates was given by Cooper and coworkers [5], considering the correlation between the optical excitations across the charge-transfer gap in $YBa_2Cu_3O_{7-x}$ and the resonant behaviour of the magnetic peak in the B_{1g} Raman response. Similar (but less pronounced) dependence on the frequency of the incident/scattered photons is also found in the Drude part of the Raman spectra. The latter is also accompanied by several anomalies regarding the relative spectral weights of three Raman polarizations. [3, 9, 10]

Actually, the recent interest in the Drude part of the optical conductivity and Raman scattering spectra of the underdoped compounds is stimulated by the clear evidence for important role of the normal-state coherence effects. The optical conductivity and B_{2g} Raman spectra scan the electronic states in the nodal region of the Fermi surface (so-called "cold spots" on the Fermi surface: $k_x = k_y$), while the A_{1g} and B_{1g} Raman scattering processes probe the electronic states in the vicinity of the van Hove points ("hot spots"). A striking difference between these two groups of spectra occurs for the nearly half filled conduction band in all cases where there is a perturbation peaked at (usually commensurate) wave vector $\mathbf{Q}$ close to the nesting vector of the Fermi surface $2\mathbf{k}_F$. The AF fluctuations at small dopings [4, 9] and the charge-density-wave (CDW) fluctuations at the 1/8 doping [8] are typical examples. There is also a surprising similarity between the mid-infrared (MIR) peak in the optical conductivity, $\hbar\omega^{\rm ir}_{\rm peak}$, and the magnetic peak in

*Fax: +385-1-4680-336,
E-mail address: kupcic@phy.hr (I. Kupčić)

the B_{1g} Raman spectra. Both appear at nearly the same energy, exhibit similar doping dependence and possibly have the same physical origin. [4, 5, 9, 10]

It is interesting also to note that in the materials where the MIR peak appears at a relatively small energy, comparable with the typical damping energy $\Sigma \equiv \hbar/\tau$ [7, 8], there is an essential difference between the predictions of the usual one-band optical models and measurements. It is explicitly shown that the development of the measured MIR structure with temperature can be fitted well with the orbital Kondo model of Emery and Kivelson [19] (representing the regime where $\hbar\omega^{\rm ir}_{\rm peak} \approx \Sigma$) rather than with the mentioned one-band models (underdamped regime: $\hbar\omega^{\rm ir}_{\rm peak}$ is proportional to characteristic correlation energy scales, such as the Hubbard interaction U [11, 12] or the AF exchange energy J [13]).

The main goal of the present analysis is the following: (i) to determine for the Emery three-band model [20] all electron-photon coupling functions (various current and Raman vertices, to be defined below) important for the understanding of most of the aforementioned anomalies, (ii) to show that, due to the gauge invariance, the present multi-component optical model allows a natural transformation of the spectra from the underdamped regime into the overdamped regime, [21] and (iii) to point out that the correlation effects peaked at $\mathbf{Q} \approx 2\mathbf{k}_{\rm F}$ (the AF correlations in the cuprates, or the umklapp scattering processes in the Bechgaard salts [21, 22, 23, 24]) affect the optical conductivity of two-dimensional (2D) and quasi-one-dimensional (Q1D) systems in a similar way, leading in both cases to the dramatic decrease of the effective number of conduction electrons.

However, to ensure a simple analytic form of the current and Raman vertices, the present analysis will be limited by the use of several approximations. (i) The effects of the AF correlations on the response functions will be included in an adiabatic way. (ii) The strong local correlations associated with the Hubbard term on the copper sites will be treated in the mean-field approximation (MFA), with the same (renormalized) copper-oxygen transfer integral describing the low- and high-frequency excitations. (iii) As usual for the in-plane features of the high-T_c cuprates, the 2D representation of the electronic system is used, neglecting several important questions dependent on the electron propagation in the direction perpendicular to the conduction planes, such as the anomalous c-axis conductivity or the dimensionality crossover.

In this paper, the response of the valence electrons in the high-T_c cuprates to the external vector potential is analyzed by means of the Emery three-band model [20]. The AF correlations in the nearly half filled conduction band are modeled by an effective single-particle interaction $\Delta(\mathbf{k})$ peaked at the commensurate wave vector $\mathbf{Q} = (\pi/a, \pi/a)$. In the calculation we adopt a gauge invariant approach which has been proved to enable a systematic study of the multi-component optical conductivity spectra [25] and which is a simple generalization of the memory-function approach [21]. It will be shown that an anisotropic-s effective interaction results in two distinct features in the low-frequency optical conductivity, with the relation between these two features and the high-frequency excitations across the *pd* charge-transfer gap which quantitatively agrees with the experimental observations (including the position of thresholds and the ratio between the respective spectral weights).

In Section 2 we describe the simplest version of the three-band model which focuses on the optical excitations across the *pd* charge-transfer gap and on the low-frequency excitations across the MIR correlation gap $2\Delta(\mathbf{k})$ (in the rest of the text the MIR conductivity related to $\Delta(\mathbf{k})$ will be referred to as the MIR gap structure), and review other work. We determine the gauge invariant form of the static and elastic Raman vertices (Appendices A and B), which makes possible the consistent formulation of both the three-component optical conductivity and the related Raman correlation functions. Section 3.1 discusses the conductivity sum rules of the present three-component optical model, while in Section 3.2 the dependence of the low-frequency spectra on the symmetry and magnitude of the effective interaction $\Delta(\mathbf{k})$ is studied. Finally, the mutually competing effects of the intracell hybridizations and the strong local correlations on the interband spectra of the lightly-doped conducting planes are briefly discussed in Section 3.3.

II. THEORETICAL MODEL

The electrodynamics of valence electrons in the high-T_c cuprates is described in terms of the extended Hubbard model (i.e. the Emery three-band model [20] in which all Coulomb interactions are neglected except for the Hubbard interaction on the copper sites U_d). As mentioned in Introduction, various one-band versions of this model have been widely used to describe qualitatively the low-frequency optical conductivity. Let us first briefly review these models. Then follow the detailed explanation of the present optical model and the comparison with the experimental data.

The theoretical study of the underdoped regime reveals the MIR gap structure in the optical conductivity, in accordance with experimental observation. In the one-band Hubbard model [11, 12] the corresponding threshold energy is proportional to the Hubbard interaction U (precisely, $\hbar\omega^{\rm ir}_{\rm peak} \approx U/2$, with an additional, charge-transfer gap at $\hbar\omega^{\rm inter}_{\rm peak} \approx U$), while in the t-J model [13] this energy is related to the AF exchange energy J. Most of the relevant results are calculated using the *numerical* diagonalization procedure at *high temperatures* (usually $T > 500$ K). Similarly, the anomalous (non-Drude, single-component) optical conductivity measured in the overdoped compounds can be explained in terms of the marginal Fermi liquid theory [1] or the nested Fermi liquid theory [2], which are characterized by strong quasiparticle damping effects. It is essential to notice that fits

of the related generalized Drude formula to the measured spectra require usually *large damping energies* (typically $\hbar/\tau(0.5\text{ eV}) \approx 0.5$ eV [2, 4]).

In order to treat both the local correlations related to U_d and the interplay between various small energy scales more accurately (at low temperatures, with presumably small damping energies), as well as to describe the relevant intracell processes explicitly, different three-band versions of the Emery model are examined and contrasted to the measured low- and high-frequency optical spectra and the related Raman spectra [17, 26, 27, 28, 29, 30, 31]. Kotliar, Lee and Read [26] have calculated the ground state energy of the electronic system self-consistently using the slave-boson procedure. They have shown that the characteristic of the low-frequency optical processes is the renormalization of the copper-oxygen bond energy t_{pd} (i.e. the copper-oxygen transfer integral, in the usual language). This renormalized bond energy is found to be strongly dependent on doping, in particular in the lightly doped region, where $t_{pd} \propto \sqrt{\delta}$ (hereafter, δ is the hole doping). In the case where $J = 0$, the MIR structure is found to be related to the renormalized splitting between the oxygen and copper site energies, Δ_{pd} (i.e. the renormalized *pd* dimerization potential) [26, 27]. However, in the complete slave-boson model [27] this scale can be associated with the AF exchange energy J as well. In both cases, the excitations across the charge-transfer gap are connected with the bare *pd* dimerization potential.

The electrodynamics of the underdoped cuprates may be close to that of the Bechgaard salts $(TMTSF)_2X$ ($X = PF_6$, ClO_4). Namely, for the nearly half filled 2D or Q1D conduction band, the SC and AF (or spin-density wave) regions in the phase diagram are expected to be controlled by small changes in the already small effective number of conduction electrons caused by the interplay between the corresponding correlation energy and various other small energy scales. [21] The measurements on the high quality crystals [22, 23] have shown that the electrodynamic features of the Bechgaard salts are strongly affected by the umklapp scattering processes, in particular by the competition between the characteristic umklapp energy and the transfer integral in the direction perpendicular to the highly conducting direction [23, 24]. In the present paper it will be proposed that the two-component low-frequency optical conductivity of the underdoped cuprates is connected with a similar correlation energy related to the AF pseudogap processes, and that the transformation of this two-component form into a single-component form, in the overdoped regime, is related with the interplay between this scale and the energy difference between the Fermi energy and the van Hove energy. By analogy with the Bechgaard salts, one should extend the present analysis by considering the competition between the characteristic AF energy and the oxygen-oxygen transfer integral t_{pp} (this is expected to be relevant for the in-plane conductivity in the lightly-doped regime), or the interplane transfer integral $t_\perp$ (important for the *c*-axis conductivity and the dimensionality crossover problem); however, these are beyond the scope of the present work.

Finally, it is important to note that the present optical conductivity analysis, together with the related Raman analysis [18], can be easily connected with the Hall coefficient measurements [32], due particularly to the analytic form of the intra- and interband current and Raman vertex functions. It should also be noticed that the model parameters extracted below from the optical data can be confirmed by angle-resolved photoemission spectroscopy (ARPES) experiments [33, 34, 35, 36, 37, 38] (the conduction band is wide and nearly half filled), as well as by electric field gradient (EFG) measurements [39, 40] (the copper-oxygen hybridization is relatively strong, again, supporting the picture of wide bands [41]).

A. Bare three-band Hamiltonian

The present response theory is based on an effective single-particle description of the valence electrons. The analysis starts with the 2D three-band Hamiltonian of the form [26, 29]

$$\begin{aligned} H_0 &= \sum_L H_0^L, \\ H_0^L &= \sum_{\mathbf{k}\sigma} E_L(\mathbf{k}) L^\dagger_{\mathbf{k}\sigma} L_{\mathbf{k}\sigma}. \end{aligned} \tag{1}$$

In the hole picture, the bonding band (the band index $L = D$) is nearly half filled, while the antibonding and nonbonding bands ($L = P$ and N) are empty.

Two versions of the model will be considered. The model A includes only two parameters, the splitting between the oxygen $2p_\sigma$ and copper $3d_{x^2-y^2}$ site energies Δ_{pd} and the average first-neighbor bond energy t_{pd}. Since two different limits of the three-band model, the $U_d = 0$ limit and the MFA of the $U_d \to \infty$ limit (hereafter, the large U_d case), are represented by this model, the parameters Δ_{pd} and t_{pd} can be associated either with the bare parameters or with the parameters renormalized by the large U_d (in the latter case, the present model is identical to the original slave-boson model of Kotliar, Lee and Read [26]). The distinction between these two situations, together with a naive phenomenological extension of the large U_d problem, will be briefly discussed in Section 3.3.

The model B focuses on the bonding band only, i.e. on an effective low-frequency description of the conduction electrons. So long as the underdoped regime is in question, the main low-frequency effects are expected to come from an opening of a correlation gap in the single-particle excitation spectrum. These effects are related here to the AF correlations and are described in the adiabatic way, by considering the influence of an effective single-particle interaction

$$H_{\text{corr}} = \sum_{\mathbf{k}\sigma} [\Delta(\mathbf{k}) D^\dagger_{\mathbf{k}\sigma} D_{\mathbf{k}\pm\mathbf{Q}\sigma} + \text{h.c.}] \tag{2}$$

on the real part of the electron self-energy, with $\mathbf{Q} = (\pi/a, \pi/a)$ being the AF wave vector. Although the effect of these correlations on the imaginary part of the electron self-energy is not treated explicitly, it can be represented by a phenomenological contribution to the damping energies which increases linearly with frequency (see a comment on the generalized Drude formula given below). The magnitude of $\Delta(\mathbf{k})$ is assumed to be real and small, as compared with the energies Δ_{pd} and t_{pd}.

The structure of the Bloch functions and the Bloch energies of the model A is well known [26, 29]. On the other hand, the diagonalization of the model B (i.e. of the Hamiltonian $H_0^D + H_{\rm corr}$) is straightforward, leading to the dimerized bonding band with the dispersions of the upper ($L = A$) and lower ($L = S$) subbands given by

$$E_{A,S}(\mathbf{k}) = \frac{1}{2}[E_D(\mathbf{k}) + E_{\underline{D}}(\mathbf{k})] \pm\sqrt{\frac{1}{4}[E_D(\mathbf{k}) - E_{\underline{D}}(\mathbf{k})]^2 + \Delta^2(\mathbf{k})}, \quad (3)$$

where $E_{\underline{D}}(\mathbf{k}) \equiv E_D(\mathbf{k} \pm \mathbf{Q})$. The effect of the perturbation $H_{\rm corr}$ on the Bloch functions is given in the usual way, in terms of the auxiliary phase $\varphi_{\mathbf{k}}$ defined in Appendix B.

B. Coupling Hamiltonian

According to Ref. [25], the coupling of the conduction electrons to the external electromagnetic fields, relevant to the in-plane optical conductivity analysis, is given by the coupling Hamiltonian

$$H^{\rm ext} = -\frac{1}{c}\sum_{LL'\mathbf{k}\sigma}[A_\alpha(\mathbf{q}_\perp)J_\alpha^{LL'}(\mathbf{k})L^\dagger_{\mathbf{k}+\mathbf{q}_\perp\sigma}L'_{\mathbf{k}\sigma} + \text{h.c.}] + \frac{e^2}{2mc^2}\sum_{\mathbf{k}\sigma}[A^2_\alpha(\mathbf{q}_\perp)(-)\gamma^{CC}_{\alpha\alpha}(\mathbf{k};2)C^\dagger_{\mathbf{k}+\mathbf{q}_\perp\sigma}C_{\mathbf{k}\sigma} + \text{h.c.}]. \quad (4)$$

Here C is the index of the conduction band ($C \equiv D$ in the model A and $C \equiv A$ in the model B), and $\alpha \in \{x, y\}$ is the photon polarization index. The $J_\alpha^{LL'}(\mathbf{k})$ are the coupling functions in the first-order term (the current vertices) and $\gamma^{CC}_{\alpha\alpha}(\mathbf{k};2)$ is the coupling function in the bare second-order term (the bare Raman vertex). Furthermore, $A_\alpha(\mathbf{q}_\perp)$ and $A^2_\alpha(\mathbf{q}_\perp)$ are the Fourier transforms in space of the vector potential $A_\alpha(\mathbf{r})$ and of its square $A^2_\alpha(\mathbf{r})$, respectively, and $\mathbf{q}_\perp \cdot \mathbf{a}_\alpha = 0$. The coupling functions of the models A and B are shown explicitly in Appendices A and B.

C. Optical conductivity

The doping dependence of the optical conductivity spectra of the $La_{2-x}Sr_xCuO_4$ single crystals has been systematically examined by Uchida et al. [4]. The underdoped crystals exhibit the behaviour which cannot be described as the response of a Drude metal. In particular, two distinct threshold energies are found in the underdoped regime. The first one (MIR threshold energy) is strongly affected by the doping level (with the maximum in the spectra at the energy $\hbar\omega^{\rm ir}_{\rm peak}$ placed between 0.1 and 0.3 eV). In the clean (underdamped) limit of the model B ($\Delta_0 \gg \Sigma_3$, where Δ_0 labels the magnitude of the parameter $\Delta(\mathbf{k})$ and Σ_3 is the MIR damping energy), this energy should be ascribed to the AF pseudogap ($E_A(\mathbf{k}_F) - E_S(\mathbf{k}_F)$, with $\mathbf{k}_F$ on the Fermi surface). In contrast to that, the aforementioned one-band models had success in explaining this structure in terms of the parameters $U/2$ [11, 12], J [13] or Σ [19]. The second (charge-transfer) gap appears at 1.5−2 eV. In the model A, this energy scale is connected with the *pd* dimerization gap ($E_L(\mathbf{k}_F) - E_D(\mathbf{k}_F)$, $L = N, P$), and, importantly, is not simply related to the MIR threshold energy.

In the gauge invariant formalism [25, 42], the optical conductivity of the underdoped high-T_c cuprates can be thus shown in the form

$$\sigma^{\rm total}_\alpha(\omega) \approx \frac{\rm i}{\omega}\frac{e^2 n_{\rm c}^{\rm eff}}{m}\frac{\hbar\omega}{\hbar\omega + {\rm i}\Sigma_1} - {\rm i}\omega\alpha^{\rm ir}_\alpha(\omega,\Sigma_3) - {\rm i}\omega\alpha^{\rm inter}_\alpha(\omega,\Sigma_2) - \frac{{\rm i}\omega}{4\pi}[\varepsilon_{\alpha,\infty}(\omega) - 1]. \quad (5)$$

The four quantities which enter into this expression represent the effective number of conduction electrons per unit volume, $n_{\rm c}^{\rm eff}$, the MIR polarizability, $\alpha^{\rm ir}_\alpha(\omega,\Sigma_3)$, the interband polarizability, $\alpha^{\rm inter}_\alpha(\omega,\Sigma_2)$, and the contribution of all other, on-site high-frequency optical processes, $\varepsilon_{\alpha,\infty}(\omega)$.

The Σ_i are three phenomenological damping energies. As pointed out above, the description of the low-frequency processes in Eq. (5) can be easily improved by extending the first term to include the frequency dependent corrections in the intraband damping energy ($\Sigma_1 \to \Sigma_1(\omega) \equiv \hbar/\tau(\omega)$, usually $\hbar/\tau(\omega) = \hbar/\tau + \alpha\hbar\omega$) and the effective mass (which frequency dependence is forced by the causality principle, $n_{\rm c}^{\rm eff}/m \to n/m(\omega)$). It should be recalled that the generalized Drude formula ($\alpha \neq 0$, but $\alpha^{\rm ir}_\alpha(\omega) = 0$ and $\alpha^{\rm inter}_\alpha(\omega) = 0$) would hardly be extended to the underdoped regime because large damping energies are required to explain measured spectra [4]. In the present analysis of the underdoped regime, where the MIR optical activity is associated with the excitations across the AF pseudogap, rather than with the strong intraband damping effects, such frequency corrections to Σ_1 are presumably small, and will be disregarded in the quantitative analysis given in Section 3.

In the model B, the first two terms in Eq. (5) are given

by

$$n_{\rm c}^{\rm eff} \;=\; \frac{1}{V}\sum_{\mathbf{k}^*\sigma}\gamma_{xx}^{AA}(\mathbf{k})[1-f_A(\mathbf{k})], \qquad (6)$$

$$\alpha_\alpha^{\rm ir}(\omega,\eta) \;=\; \frac{1}{\omega^2}\frac{1}{V}\sum_{\mathbf{k}^*\sigma}\frac{(\hbar\omega)^2|J_\alpha^{AS}(\mathbf{k})|^2}{E_{AS}^2(\mathbf{k})} \times\frac{2E_{AS}(\mathbf{k})[f_A(\mathbf{k})-1]}{(\hbar\omega+{\rm i}\eta)^2-E_{AS}^2(\mathbf{k})}. \qquad (7)$$

The sum $\sum_{\mathbf{k}^*}$ is restricted to the first Brillouin zone of the dimerized lattice, and $\gamma_{xx}^{AA}(\mathbf{k})$ is the static Raman vertex defined in Appendix B. Similarly, the model A gives rise to the interband polarizability of the form

$$\alpha_\alpha^{\rm inter}(\omega,\eta) \;=\; \frac{1}{\omega^2}\frac{1}{V}\sum_{\mathbf{k}\sigma L\neq D}\frac{(\hbar\omega)^2|J_\alpha^{LD}(\mathbf{k})|^2}{E_{LD}^2(\mathbf{k})} \times\frac{-2E_{LD}(\mathbf{k})f_D(\mathbf{k})}{(\hbar\omega+{\rm i}\eta)^2-E_{LD}^2(\mathbf{k})}. \qquad (8)$$

The Fermi-Dirac function $[1+e^{\beta[E_L(\mathbf{k})-\mu]}]^{-1}$ is denoted by $f_L(\mathbf{k})$, and the energy difference $E_L(\mathbf{k})-E_{L'}(\mathbf{k})$ by $E_{LL'}(\mathbf{k})$.

Since the contribution of the on-site high-frequency processes is nearly independent of doping, and is small at energies below 3 eV, we take $Im\{\varepsilon_{\alpha,\infty}(\omega)\}=0$ and $Re\{\varepsilon_{\alpha,\infty}(\omega)\}\approx\varepsilon_\infty$ in this energy region. (A better approximation for $\varepsilon_{\alpha,\infty}(\omega)$ is given at the end of the article.) For further considerations it is appropriate to denote the first three contributions in Eq. (5) by $\sigma_\alpha^{\rm Drude}(\omega)$, $\sigma_\alpha^{\rm ir}(\omega)$ and $\sigma_\alpha^{\rm inter}(\omega)$, with the abbreviation $\sigma_\alpha^{\rm intra}(\omega)\equiv\sigma_\alpha^{\rm Drude}(\omega)+\sigma_\alpha^{\rm ir}(\omega)$.

The corresponding macroscopic dielectric function reads as

$$\varepsilon_\alpha(\omega) \;=\; 1+\frac{4\pi{\rm i}}{\omega}\sigma_\alpha^{\rm total}(\omega), \qquad (9)$$

giving finally the three-component optical model with the minimal number of adjustable parameters: t_{pd}, Δ_{pd}, Δ_0, Σ_i and ε_∞. (Actually, we take over the estimate of the ratio t_{pd}/Δ_{pd} from the EFG analysis [41], and reduce additionally the number of independent model parameters.)

III. RESULTS AND DISCUSSION

Let us remember some additional details about the optical anomalies of the underdoped and lightly-doped $La_{2-x}Sr_xCuO_4$ crystals. (i) A small transfer of the spectral weight across the charge-transfer gap is observed with decreasing doping in the $0.2>\delta>0.1$ doping region (the derivative $\partial\Omega_{\rm inter}^2/\partial\delta$ is negative but small; $\Omega_{\rm inter}^2$ is the interband spectral weight to be defined below). (ii) As mentioned above, this phenomenon is accompanied by the appearance of the MIR peak placed at $\hbar\omega_{\rm peak}^{\rm ir}\approx 0.1$ eV. (iii) The additional decrease of doping, below $\delta<0.1$, is characterized by a dramatic increase of the spectral weight above the charge-transfer gap (i.e. $\partial\Omega_{\rm inter}^2/\partial\delta<0$ becomes large, resulting for $\delta\approx 0$ in the complete disappearance of the intraband spectral weight). (iv) The MIR peak is also shifted, resulting in $\hbar\omega_{\rm peak}^{\rm ir}\approx 0.15$ eV and $\hbar\omega_{\rm peak}^{\rm ir}\approx 0.3$ eV at $\delta=0.1$ and $\delta=0.06$, respectively.

These features will be discussed now in the framework of the present three-component optical model. The considerations include three important questions. First, starting from the model parameters independent of doping, we show how the total spectral weight is shared among the Drude, MIR and interband channels. Second, we illustrate the dependence of the low-frequency optical conductivity on the symmetry and magnitude of AF pseudogap. Finally, the validity of the model (5)−(8) in the lightly doped regime is tested on comparing the experimental spectra measured at $\hbar\omega<3$ eV to the ones which correspond to the model parameters independent of doping. The characteristic energy scales used in the numerical calculations, $\Delta_{pd}=0.66$ eV and $t_{pd}=0.73$ eV, are deduced from the estimate of the intracell hybridization $t_{pd}/\Delta_{pd}\approx 1.1$ [41] obtained on the basis of the intracell charge distributions measured in the $La_{2-x}Sr_xCuO_4$ compounds by the EFG probes, and by assuming that the charge-transfer energy is roughly equal to 1.75 eV for the doping level $\delta=0.2$.

A. Conductivity sum rules

There has been a lot of interest in the sum rules of the high-T_c cuprates, in particular in the c-axis conductivity sum rule and the in-plane Pines-Noziéres sum rule [42, 43], both of which exhibit an indirect, relatively complicated dependence on the MIR threshold energy. Since it is not a trivial task in the three-band model to determine these sum rules, the related theoretical analyses have employed again the numerical treatments of the one-band models or suitable phenomenological models [14, 15, 16]. This contrasts with the direct dependence of the in-plane conductivity sum rule of the underdoped compounds on both the MIR and charge-transfer threshold energy, where it is possible to make a relatively simple estimation of the model parameters, in particular their dependence on the doping level. Let us now examine the latter issue in more detail.

The experimental analyses present usually the total spectral weight of $\sigma_\alpha^{\rm total}(\omega)$ in terms of the spectral function $N_{\rm eff}(\hbar\omega)$ defined by [4, 5]

$$N_{\rm eff}(\hbar\omega) \;=\; \frac{8}{\Omega_0^2}\int_0^\omega {\rm d}\omega'\; Re\{\sigma_\alpha^{\rm total}(\omega')\}. \qquad (10)$$

The frequency $\Omega_0=\sqrt{4\pi e^2/(mV_0)}$ is a frequency-scale parameter, and V_0 is the primitive cell volume.

Alternatively, in the multi-component optical models, several auxiliary frequencies, together with the associated effective numbers, can be defined by considering the

spectral weight contained by the i-th channel

$$\Omega_i^2 = 4\int_{-\infty}^{\infty} \mathrm{d}\omega\ Re\{\sigma_\alpha^i(\omega)\} \equiv V_0 n_i^{\mathrm{eff}} \Omega_0^2. \quad (11)$$

(To simplify notation, we will refer to Ω_i^2 as the spectral weight in the i-th channel. Obviously, this differs from the usual normalization of the spectral weight by a factor 1/2.) The index $i \in$ {total, intra, inter, Drude, ir}. Notice that $n_{\mathrm{Drude}}^{\mathrm{eff}}$, defined by this relationship, is identical to $n_{\mathrm{c}}^{\mathrm{eff}}$ in Eq. (5).

The conductivity sum rules of the present optical models A and B are most appropriately described by

$$\Omega_{\mathrm{total},0}^2 = \Omega_{\mathrm{intra},0}^2 + \Omega_{\mathrm{inter},0}^2, \quad (12)$$

$$\Omega_{\mathrm{intra}}^2 = \Omega_{\mathrm{Drude}}^2 + \Omega_{\mathrm{ir}}^2 \quad (13)$$

(the label 0 in Eq. (12) refers to $\Delta(\mathbf{k}) = 0$). For the narrow bands with the relaxation processes negligible (limit $\Sigma_i \to 0$), the spectral function $N_{\mathrm{eff}}(\hbar\omega)$ has a step-like form, with the steps simply related to Eqs. (12) and (13). However, in the typical experimental situations (where the bands are wide and the damping energies are not negligible) the relationship between these two representations of the total spectral weight is more complicated (see Eqs. (16)). Nevertheless, a careful comparison between the measured spectral functions $N_{\mathrm{eff}}(\hbar\omega)$ and the analytic expressions for Ω_i^2 can be used to extract the values of the parameters involved in the model (5), or in some more general optical model (see Ref. [44], where the intraband spectral weight and the related effective number of electrons are estimated in various optimally doped cuprates and correlated with T_c).

Shown in Fig. 1, the data $N_{\mathrm{eff}}(3\mathrm{eV})$ measured in $La_{2-x}Sr_xCuO_4$ and the total spectral weight of the three-band model,

$$\Omega_{\mathrm{total},0}^2 = \Omega_0^2 \frac{1}{N}\sum_{\mathbf{k}\sigma}(-)\gamma_{\alpha\alpha}^{DD}(\mathbf{k};2) f_D(\mathbf{k}), \quad (14)$$

display the same doping dependence. At the same time, the doping dependence of the intraband spectral weight is given by

$$\Omega_{\mathrm{intra},0}^2 = \Omega_0^2 \frac{1}{N}\sum_{\mathbf{k}\sigma}(-)\gamma_{\alpha\alpha}^{DD}(\mathbf{k}) f_D(\mathbf{k}). \quad (15)$$

The intra- and interband spectral weights are also shown in Fig.1. Interestingly, due to the gauge invariant form of $\sigma_\alpha^{\mathrm{total}}(\omega)$, none of these three spectral weights depends on the damping energies. (Here $\gamma_{\alpha\alpha}^{DD}(\mathbf{k})$ is the static Raman vertex of the model A; see the effective mass theorem (A3)).

It should also be recalled that this figure shows the results obtained in the simplest case, in which the parameters Δ_{pd} and t_{pd} are assumed to be independent of doping. In this case, for the doping range relevant to the hole-doped high-T_c cuprates, $0 < \delta < 0.3$, the calculated total spectral weight is shared between the intra- and interband channels nearly in equal proportions.

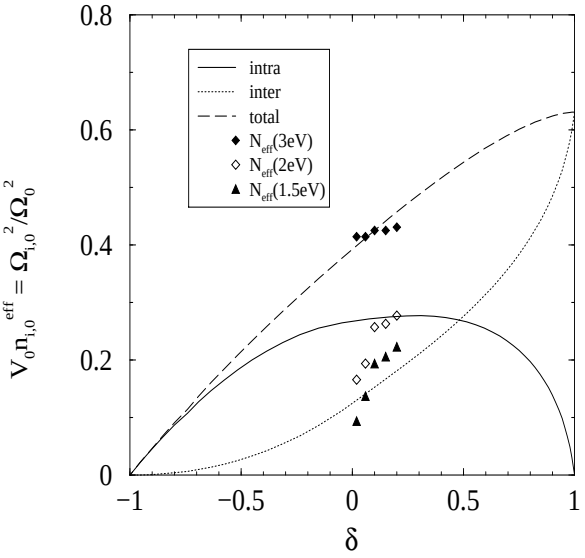

FIG. 1: The effective number of electrons in the model A as a function of the hole doping. The experimental points $N_{\mathrm{eff}}(1.5\mathrm{eV})$ (filled triangles), $N_{\mathrm{eff}}(2\mathrm{eV})$ (open diamonds) and $N_{\mathrm{eff}}(3\mathrm{eV})$ (filled diamonds) measured in $La_{2-x}Sr_xCuO_4$ (Ref. 4, with $\delta = x$ assumed) are also shown.

Fit of the predicted spectral weights to the measured data is based on the relationships

$$\Omega_{\mathrm{total},0}^2 \approx N_{\mathrm{eff}}(\hbar\omega_{\max})\Omega_0^2,$$
$$\Omega_{\mathrm{intra},0}^2 \approx N_{\mathrm{eff}}(\hbar\omega_{\min})\Omega_0^2. \quad (16)$$

Here $\hbar\omega_{\max}$ and $\hbar\omega_{\min}$ are the effective maximal and minimal energy in the interband processes, respectively. Although there is a large inaccuracy in the experimental determination of $\hbar\omega_{\min}$ and $\hbar\omega_{\max}$, it seems that $0.2 < N_{\mathrm{eff}}(\hbar\omega_{\min}) < 0.25$ and $N_{\mathrm{eff}}(\hbar\omega_{\max}) \approx 0.5$ almost in all La_2CuO_4 based compounds [4, 5, 6] (see, for example, Fig. 10 in Ref. [4]). In this respect, note that the MFA of the large U_d case (i.e. for the average bond energy involved both in the low- and high-frequency processes), together with the conclusions of the EFG analysis, suggests the cutoff energy $\hbar\omega_{\min} \approx 2$ eV (Fig. 1), contrary to the experimental optical studies, which are consistent in the conclusion that $\hbar\omega_{\min} < 1.5$ eV. In Section 3.3 we will turn to a more detailed discussion of this discrepancy.

In the model B, one obtains that the spectral weight of the MIR processes is given by

$$\Omega_{\mathrm{ir}}^2 = \Omega_0^2 \frac{1}{N}\sum_{\mathbf{k}^*\sigma}\frac{m}{e^2}\frac{2|J_\alpha^{AS}(\mathbf{k})|^2}{E_{AS}(\mathbf{k})}[1 - f_A(\mathbf{k})], \quad (17)$$

and that of the Drude term by

$$\Omega_{\mathrm{Drude}}^2 = V_0 n_{\mathrm{c}}^{\mathrm{eff}} \Omega_0^2. \quad (18)$$

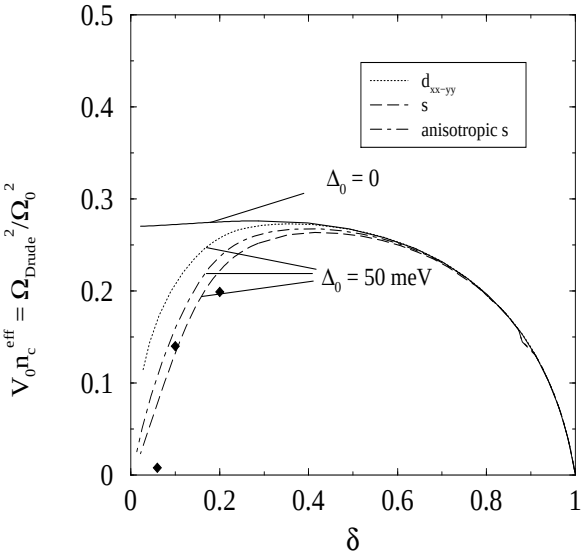

FIG. 2: The dependence of the Drude spectral weight on the symmetry of the AF pseudogap in the hole doped regime, for $\Delta_0 = 50$ meV. The filled diamonds represent the square of the measured plasma frequency [4] shown in units of $\Omega_0^2/\varepsilon_\infty$, as discussed in the text. The parameters are $\hbar\Omega_0 \approx 3.8$ eV and $\varepsilon_\infty \approx 5$.

The resulting doping dependence of the Drude spectral weight is illustrated in Fig. 2, for three symmetries of the effective potential

$$\begin{aligned} \Delta(\mathbf{k}) &= \Delta_0, \\ \Delta(\mathbf{k}) &= \frac{1}{2}\Delta_0(\cos\mathbf{k}\cdot\mathbf{a}_1 - \cos\mathbf{k}\cdot\mathbf{a}_2), \\ \Delta(\mathbf{k}) &= \Delta_0\sqrt{\frac{1}{2} + \frac{1}{8}(\cos\mathbf{k}\cdot\mathbf{a}_1 - \cos\mathbf{k}\cdot\mathbf{a}_2)^2}, \end{aligned} \quad (19)$$

corresponding, respectively, to the AF pseudogap of the s, $d_{x^2-y^2}$ and anisotropic-s symmetry. Again, $t_{pd} = 0.73$ eV is the average bond energy, and both spectral weights are independent of Σ_i.

The most noticeable feature of the Drude spectral weight is the occurrence of two different metallic behaviors: (i) the electron-like behavior characterized by $\partial\Omega_{\rm Drude}/\partial\delta < 0$, and (ii) the hole-like behavior where $\partial\Omega_{\rm Drude}/\partial\delta > 0$. For $\Delta_0 \ll t_{pd}, \Delta_{pd}$, the critical doping δ_0, at which the behavior of the conduction electrons will be changed, is only weakly dependent on the AF pseudogap symmetry. The critical doping associated with the curves in Fig. 2 agrees well with the results of the Hall effect measurements (where the sign reversal of the Hall coefficient is found at $\delta_0 \approx 0.25$ [4, 32]).

Finally, one can also notice that, when the doping level is reduced well below δ_0, the effective number of charge carriers obtained by the expression (6) can be adequately described by the free-hole approximation. The effective number of holes is small with respect to the number of electrons in the conduction band, $(1-\delta)/V_0$. Eq. (18), together with the definition of the static Raman vertex, is the relevant expression to reconcile the concept of large Fermi surfaces, supported by the ARPES experiments, with the small effective number of holes, estimated from the Drude spectral weight or from the associated electron plasma frequency (the measured plasma frequencies are indicated in Fig. 2, using a simplified single-band expression $\Omega^2_{\rm Drude} \approx \varepsilon_\infty(\Omega^2_{\rm pl} + 1/\tau^2) \approx \varepsilon_\infty\Omega^2_{\rm pl}$).

B. Low-frequency optical conductivity

According to Fig. 2, the above description of the MIR correlations becomes ineffective for the magnitude Δ_0 small in comparison with the energy difference between the Fermi energy and the van Hove energy, $\mu - \varepsilon_{vH}$. In such circumstances, the two-component low-frequency optical conductivity, characterized by the distinct MIR threshold energy, will transform into a nearly single-component form with the increasing role of the frequency dependent corrections to the intraband damping energy [1, 2, 28]. Not surprisingly, these qualitative changes in the spectra are correlated with the sign reversal of the Hall coefficient [18].

In order to express the dependence of the low-frequency optical conductivity on the model parameters more clearly, we show in Fig. 3 the normalized spectra for a few characteristic cases. First, it should be recalled that the intraband spectral weight is directly dependent on the electron group velocity $J^{DD}_\alpha(\mathbf{k})/e$, namely $\Omega^2_{\rm intra,0} = V_0 n^{\rm eff}_{\rm intra}\Omega_0^2$ and

$$n^{\rm eff}_{\rm intra} = \frac{m}{e^2}\frac{1}{V}\sum_{\mathbf{k}\sigma}[J^{DD}_\alpha(\mathbf{k})]^2\delta[E_D(\mathbf{k}) - \mu]. \quad (20)$$

As a result, the transfer of the spectral weight across the MIR gap will be strongly enhanced by the s component of the parameter $\Delta(\mathbf{k})$. However, a huge MIR peak has never been observed in $La_{2-x}Sr_xCuO_4$ or in La_2CuO_{4+x} measured spectra (for example, compare the relative intensity of the MIR spectrum measured in $La_2CuO_{4.12}$, the long-dashed line in Fig. 3(b), with the model prediction for $\Delta(\mathbf{k}) = \Delta_0$, the long-dashed line in Fig. 3(a)). Therefore, it seems that $\Delta(\mathbf{k})$ is dominantly of the $d_{x^2-y^2}$ character, with a small s component directly related to the velocity ratio $1/(1+\lambda)$ measured in the ARPES in the nodal ($k_x = k_y$) region of the Fermi surface [34, 35, 36]. Second, in the present model, where the second-neighbor bond-energy t_{pp} is set to zero, the anomalous shift of the MIR peak structure with decreasing doping can only be understood as a result of the doping dependent magnitude Δ_0. The lower doping, the stronger effective perturbation has to be, in full agreement with the conclusion of a similar single-band analysis focused on the characteristic AF energy, given in Ref. [45], and with the related specific heat measurements [46]. A significant deviation from such doping dependence of Δ_0 is expected for t_{pp} comparable to t_{pd}, or for $t_{pp} \approx \Delta_0 > \mu - \varepsilon_{vH}$. The

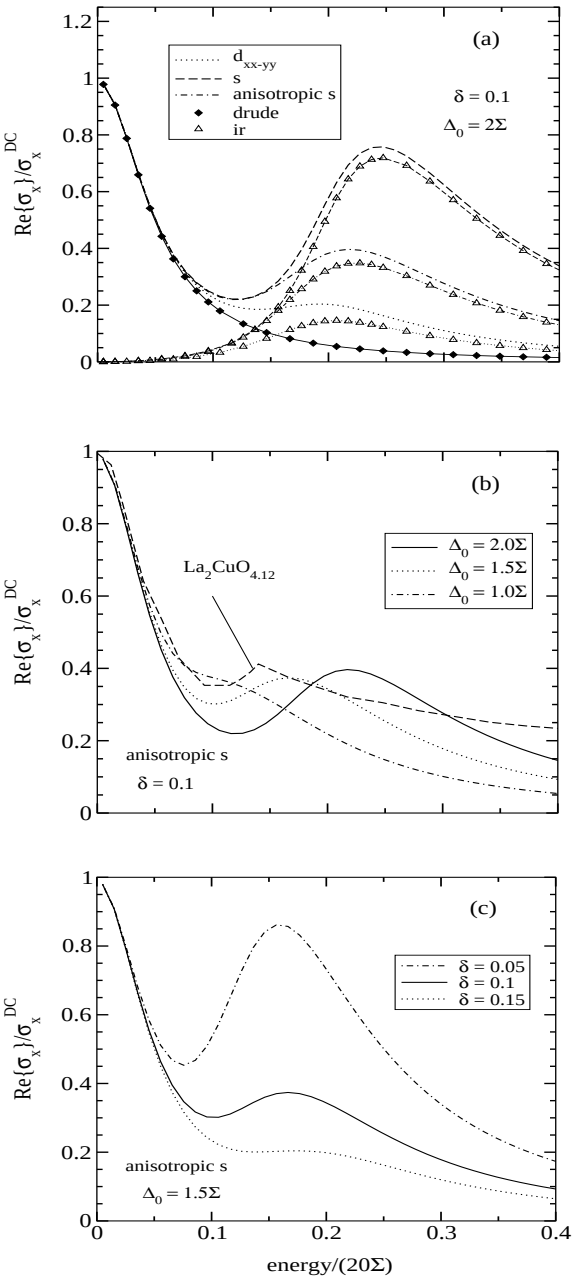

FIG. 3: The dependence of the normalized low-frequency optical conductivity on the AF pseudogap symmetry (a) and magnitude (b), and on the doping level (c), $\Sigma_1 = \Sigma_3 = \Sigma$. $\sigma_x^{\rm DC} = \hbar\Omega^2_{\rm Drude}/(4\pi\Sigma)$ is the DC conductivity. The experimental data measured in $La_2CuO_{4.12}$ (long-dashed line in Fig. (b)) [6] are given for comparison. In this material, $\hbar\omega^{\rm ir}_{\rm peak} \approx 90$ meV and $\Sigma \approx 30$ meV at $T \approx 200$ K.

difference in the shape of the Fermi surface between the model prediction for $t_{pp} = 0$ and the experimental findings can also be removed in this more realistic case. The low-frequency optical analysis of this interesting and experimentally relevant situation will be given later.

C. Interband optical conductivity

It is interesting to investigate finally how the expression (5) relates to the interband optical conductivity data measured in the lightly-doped and underdoped compounds. Note that both the $U_d = 0$ case and the MFA of the large U_d case are unable to explain the anomalous doping dependence of the interband spectral weight (compare the model prediction for $\Omega^2_{\rm inter}$ with $N_{\rm eff}(3{\rm eV}) - N_{\rm eff}(1.5{\rm eV})$ in Fig. 1). Also, when fitted with $\Delta_{pd} = 0.66$ eV and $t_{pd} = 0.73$ eV, the model (5) underestimates the interband spectral weight of the considered compounds nearly by a factor $N_{\rm eff}(2{\rm eV})/N_{\rm eff}(1.5{\rm eV})$. The solution of the problem comes on noting that the MFA of the large U_d case treats the effects of strong local correlations on the bond energies in an average fashion. It is possible, however, to make a simple phenomenological extension of the present multiband optical model, and to improve the overall agreement between the model predictions and the measured data. This is due to the gauge invariant form of Eqs. (5)−(8), which provides a successful separation of the twofold role of the intermediate states in the optical processes. For example, the copper-oxygen hopping processes participating in the low-frequency optical activity are accompanied by $\omega = 0$ and $\Sigma_2 = 0$, resulting in the effective mass theorem (A3), in full agreement with the longitudinal multiband response theory [29]. Similarly, the high-frequency optical processes can be described in terms of the elastic Raman vertices (compare the interband polarizability with the difference $\gamma^{DD}_{\alpha\alpha}(\mathbf{k},\omega) - \gamma^{DD}_{\alpha\alpha}(\mathbf{k})$ in Eq. (A4)), with the DC conductivity behaving correctly in the metal-to-insulator phase transitions [25].

The parameters describing the low-frequency (high-frequency) optical processes in the strongly correlated systems are (are not) appreciably affected by the strong local correlations. The quantity that describes these effects is the probability of the photon absorption/emission, in the low-frequency processes given by the current vertex $\tilde{J}^{DD}_\alpha(\mathbf{k})$, in the high-frequency processes by $\tilde{J}^{DL}_\alpha(\mathbf{k})$. In the strongly correlated regime, these two vertices should be written in the form $\tilde{J}^{DD}_\alpha(\mathbf{k}) \approx t^U_{pd}/t_{pd} J^{DD}_\alpha(\mathbf{k})$ and $\tilde{J}^{DL}_\alpha(\mathbf{k}) \approx t^0_{pd}/t_{pd} J^{DL}_\alpha(\mathbf{k})$, in the first approximation. Here t^0_{pd} is the bare bond energy, t^U_{pd} is the bond energy renormalized by the large U_d, t_{pd} is the average energy used in previous sections, and $J^{LL'}_\alpha(\mathbf{k})$ are given by the expressions (A1). Consequently, the optical conductivity of the large U_d case is more appropriately described by

$$\tilde{\sigma}^{\rm total}_\alpha(\omega) \;\approx\; \sum_i \tilde{\sigma}^{\rm i}_\alpha(\omega), \tag{21}$$

where

$$\begin{aligned} \tilde{\sigma}^{\rm intra}_\alpha(\omega) &\approx (t^U_{pd}/t_{pd})^2 \sigma^{\rm intra}_\alpha(\omega), \\ \tilde{\sigma}^{\rm inter}_\alpha(\omega) &\approx (t^0_{pd}/t_{pd})^2 \sigma^{\rm inter}_\alpha(\omega), \end{aligned} \tag{22}$$

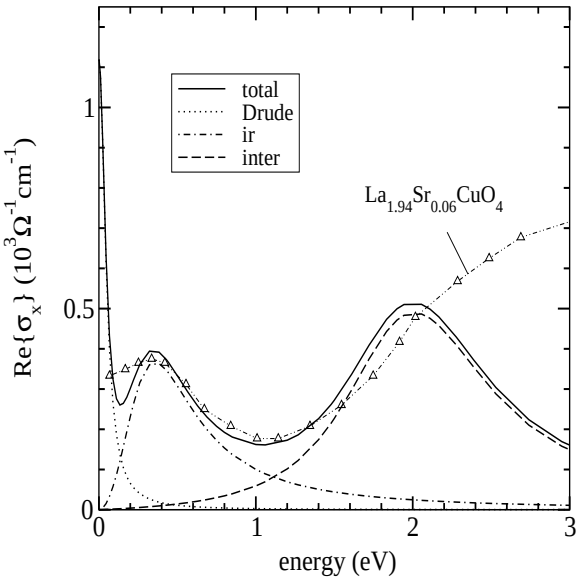

FIG. 4: The real part of the optical conductivity for $\delta = 0.06$, the $d_{x^2-y^2}$-symmetry AF pseudogap with $\Delta_0 = 0.125$ eV, $\Sigma_1 = 50$ meV, $\Sigma_2 = 0.5$ eV, $\Sigma_3 = 0.25$ eV, $\zeta_1 = 0.2$, $\zeta_2 = 1.9$ and $\zeta_3 = 0.8$. The experimental data (open triangles) are from Ref. [4].

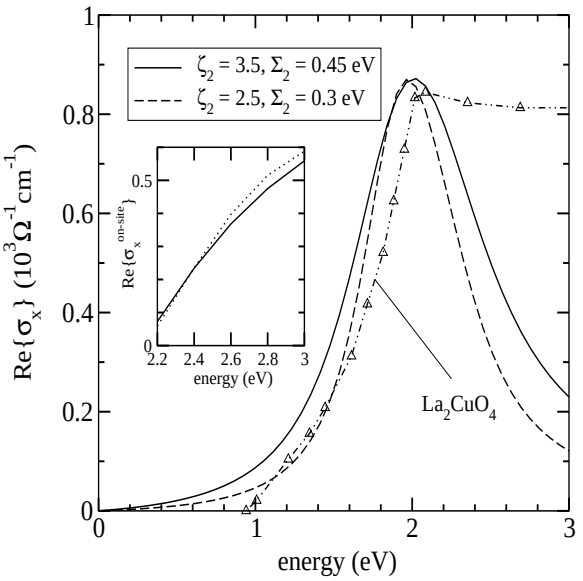

FIG. 5: Main figure: The real part of the optical conductivity at various ζ_2 for $\delta \approx 0$ and $\zeta_1 = \zeta_3 = 0$, compared with the experimental data (open triangles) [4]. Inset of figure: The on-site contributions to the optical conductivity $\omega/(4\pi) Im\{\varepsilon_{\alpha,\infty}(\omega)\}$ (i.e. the three-band-model contributions subtracted from the experimental spectra) for $\delta = 0.06$ (solid line) and $\delta = 0$ (dotted line).

or generally

$$\tilde{\sigma}^{\rm i}_\alpha(\omega) \;\approx\; \zeta_i \sigma^{\rm i}_\alpha(\omega). \tag{23}$$

ζ_1, ζ_2, and ζ_3 are three additional parameters attributed to the Drude, interband and MIR channels, respectively.

To conclude, due to insufficient information regarding the low-frequency part of the experimental spectra in the lightly-doped crystals, the discrepancy between the model predictions with the average bond-energy t_{pd} and the measured data is more clearly seen for the interband spectral weight. Its anomalous doping dependence can be understood as a result of a modification of the bond-energy renormalizations described by the factor $\zeta_2 \approx (t^0_{pd}/t_{pd})^2$ in Eqs. (21)−(23). A reasonable agreement of the data measured in the lightly-doped crystals, shown in Figs. 4 and 5, with the model (23) is achieved for $\zeta_2 \approx 2$ ($\delta = 0.06$) and $\zeta_2 \approx 3$ ($\delta = 0$). (For comparison, the value $\zeta_2 \approx 1.3$ is obtained by fitting the interband spectrum of $La_{1.8}Sr_{0.2}CuO_4$ to the model (22).) Not surprisingly, similar doping dependence of the bond-energy renormalizations is found in the previous slave-boson analyses [27, 47]. For example, for the intracell hybridization $t^U_{pd}/\Delta_{pd} = 1.1$, one obtains $(t^0_{pd}/t^U_{pd})^2 \approx 3.5$ [47], in a qualitative agreement with the present conclusions.

Obviously, for the low-frequency part of the spectra, this is an oversimplified view, because the effects of the strong local correlations on these processes are unlikely to be described simply by multiplying the MFA spectra by the factors ζ_1 and ζ_3. To clarify this essential question, further experiments in different high-T_c families are desired as a function of the doping level and with a better resolution of the low-frequency part of the spectra. Theoretically, one needs more accurate investigation of the relations between the low-frequency optical conductivity and the Raman and ARPES spectra.

Finally, notice that the difference between the experimental spectra and the conductivity $\tilde{\sigma}^{\rm total}_\alpha(\omega)$ at energies higher then 2 eV can be ascribed to the on-site interband optical conductivity $Re\{\sigma^{\rm on-site}_\alpha(\omega)\} = \omega/(4\pi) Im\{\varepsilon_{\alpha,\infty}(\omega)\}$. The on-site spectra deduced from the experimental data and the three-band model spectra (solid lines in Fig. 4 and 5) are shown in the inset of Fig. 5, for the cutoff energy $\hbar\omega_{\rm max} \approx 3$ eV, and for $\delta = 0$ and 0.06. The nearly identical frequency dependence of $Re\{\sigma^{\rm on-site}_\alpha(\omega)\}$ for these two doping levels gives an additional, although rough support to the picture of the interband optical conductivity discussed above.

IV. CONCLUSION

In this article, the influence of two dimerization potentials on the optical response of the valence electrons in the high-T_c cuprates has been studied, starting from the model parameters independent of doping. It is found that for the nearly half filled conduction band the *pd* dimerization potential leads to the spectral weights of the intra- and interband channels nearly equal to each other. It is also shown that at optimum doping the effective correlation potential related to the AF pseudogap processes results in the non-Drude nearly single-

component low-frequency optical conductivity. It is argued that, due to the decrease in the effective number of conduction electrons, the low-frequency conductivity transforms naturally from a single-component into a two-component structure with decreasing doping. Both of these results are found to be in accordance with experimental observation in the lightly-doped and underdoped La_2CuO_4 based compounds. In the present model (where the bond energy t_{pp} is set to zero), the pronounced doping dependence of the MIR peak structure is attributed to the doping dependent magnitude of the characteristic AF energy. Finally, the substantial increase of the interband spectral weight at small doping levels is interpreted in the framework of the conductivity sum rules as an indirect evidence on the strong renormalizations of the parameters describing the low-frequency physics.

Acknowledgements

Useful discussions with Professor S. Barišić are gratefully acknowledged. This work was supported by the Croatian Ministry of Science under the project 0119-256.

APPENDIX A: COUPLING FUNCTIONS IN THE MODEL A

By using the auxiliary functions $u_{\mathbf{k}}$, $v_{\mathbf{k}}$ and $t_{\mathbf{k}}$ defined in Ref. [29], one obtains that the coupling functions relevant to the case of the nearly half filled bonding band are

$$\begin{aligned} J_\alpha^{DD}(\mathbf{k}) &= \frac{eat_{pd}^2}{\hbar}\frac{2u_{\mathbf{k}}v_{\mathbf{k}}}{t_{\mathbf{k}}}\sin\mathbf{k}\cdot\mathbf{a}_\alpha, \\ J_\alpha^{DP}(\mathbf{k}) &= \frac{eat_{pd}^2}{\hbar}\frac{u_{\mathbf{k}}^2-v_{\mathbf{k}}^2}{t_{\mathbf{k}}}\sin\mathbf{k}\cdot\mathbf{a}_\alpha, \\ J_x^{DN}(\mathbf{k}) &= \frac{eat_{pd}^2}{\hbar}\frac{2u_{\mathbf{k}}}{t_{\mathbf{k}}}\sin\frac{1}{2}\mathbf{k}\cdot\mathbf{a}_2\cos\frac{1}{2}\mathbf{k}\cdot\mathbf{a}_1, \\ J_y^{DN}(\mathbf{k}) &= -\frac{eat_{pd}^2}{\hbar}\frac{2u_{\mathbf{k}}}{t_{\mathbf{k}}}\sin\frac{1}{2}\mathbf{k}\cdot\mathbf{a}_1\cos\frac{1}{2}\mathbf{k}\cdot\mathbf{a}_2, \end{aligned} \quad \text{(A1)}$$

and

$$\gamma_{\alpha\alpha}^{DD}(\mathbf{k};2) = \frac{m}{m_{xx}}\frac{\Delta_{pd}u_{\mathbf{k}}v_{\mathbf{k}}}{t_{\mathbf{k}}}\sin^2\frac{1}{2}\mathbf{k}\cdot\mathbf{a}_\alpha. \quad \text{(A2)}$$

The mass scale has the usual form $m_{xx} = \hbar^2\Delta_{pd}/(2a^2t_{pd}^2)$, with $|\mathbf{a}_1| = |\mathbf{a}_2| = a$.

By comparing two expressions for the dimensionless static Raman tensor obtained in the static limit of the longitudinal [29] and transverse response of the model A, we can verify the effective mass theorem

$$\begin{aligned} \gamma_{\alpha\alpha}^{DD}(\mathbf{k}) &= (-)\frac{m}{\hbar^2}\frac{\partial^2 E_D(\mathbf{k})}{\partial k_\alpha^2} \\ &= \gamma_{\alpha\alpha}^{DD}(\mathbf{k};2) + \frac{m}{e^2}\sum_{L=P,N}\frac{2|J_\alpha^{LD}(\mathbf{k})|^2}{E_{LD}(\mathbf{k})}. \end{aligned} \quad \text{(A3)}$$

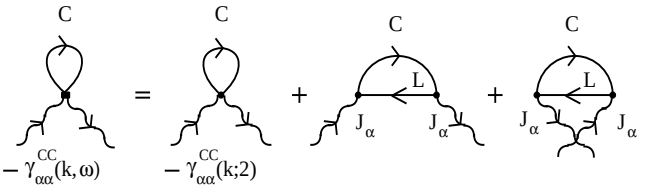

FIG. 6: The usual diagrammatic representation of the elastic Raman vertex, $L \neq C$. In the static limit of the model A (the index $C \equiv D$), the summation gives the expression (A3), i.e. the inverse $\mathbf{k}$-dependent effective mass. The wavy and solid lines represent, respectively, the photon and electron Green functions. Notice the minus sign in front of the Raman vertices which reflects the fact that electron-like conduction band is shown in the hole picture.

The related inverse $\mathbf{k}$-dependent effective mass reads as

$$(1/m)\gamma_{\alpha\alpha}^{DD}(\mathbf{k}).$$

Beyond the static approximation, the effective second-order term in the electron-photon coupling comes from the contributions shown in Fig. 6. The elastic Raman vertex is the vertex function in such effective processes. The gauge invariant form of the elastic Raman vertex reads as

$$\begin{aligned} \gamma_{\alpha\alpha}^{DD}(\mathbf{k},\omega) &= \gamma_{\alpha\alpha}^{DD}(\mathbf{k}) - \frac{m}{e^2}\sum_{L=P,N}\frac{(\hbar\omega)^2|J_\alpha^{LD}(\mathbf{k})|^2}{E_{LD}^2(\mathbf{k})} \\ &\quad\times\frac{2E_{LD}(\mathbf{k})}{(\hbar\omega+\mathrm{i}\eta)^2 - E_{LD}^2(\mathbf{k})}. \end{aligned} \quad \text{(A4)}$$

It should be noted that the usual form of the elastic Raman vertex [30, 48, 49] comes on disregarding the factor $(\hbar\omega)^2/E_{LD}^2(\mathbf{k})$ in the expression (A4).

APPENDIX B: COUPLING FUNCTIONS IN THE MODEL B

The influence of the perturbation H_{corr} on the Bloch functions can be shown in terms of the auxiliary phase which satisfies the relations

$$\begin{aligned} \cos\varphi_{\mathbf{k}} &= \frac{E_D(\mathbf{k}) - E_{\underline{D}}(\mathbf{k})}{E_{AS}(\mathbf{k})}, \\ \sin\varphi_{\mathbf{k}} &= \frac{2\Delta(\mathbf{k})}{E_{AS}(\mathbf{k})}. \end{aligned} \quad \text{(B1)}$$

The resulting static Raman vertex, the elastic Raman vertex, and the current vertices relevant to the $0 \leq \delta \leq 1$

doping range are given by

$$\gamma^{AA}_{\alpha\alpha}(\mathbf{k}) = \gamma^{DD}_{\alpha\alpha}(\mathbf{k})\cos^2\frac{\varphi_{\mathbf{k}}}{2} + \gamma^{\underline{D}\,\underline{D}}_{\alpha\alpha}(\mathbf{k})\sin^2\frac{\varphi_{\mathbf{k}}}{2} - \frac{m}{e^2}\frac{2|J^{AS}_{\alpha}(\mathbf{k})|^2}{E_{AS}(\mathbf{k})} \approx \gamma^{DD}_{\alpha\alpha}(\mathbf{k})\cos\varphi_{\mathbf{k}} - \frac{m}{e^2}\frac{2|J^{AS}_{\alpha}(\mathbf{k})|^2}{E_{AS}(\mathbf{k})}, \quad \text{(B2)}$$

$$\gamma^{AA}_{\alpha\alpha}(\mathbf{k},\omega) = \gamma^{AA}_{\alpha\alpha}(\mathbf{k}) + \frac{m}{e^2}\frac{(\hbar\omega)^2|J^{AS}_{\alpha}(\mathbf{k})|^2}{E^2_{AS}(\mathbf{k})} \times\frac{2E_{AS}(\mathbf{k})}{(\hbar\omega+\mathrm{i}\eta)^2 - E^2_{AS}(\mathbf{k})}, \quad \text{(B3)}$$

and

$$J^{AA}_{\alpha}(\mathbf{k}) = J^{DD}_{\alpha}(\mathbf{k})\cos^2\frac{\varphi_{\mathbf{k}}}{2} + J^{\underline{D}\,\underline{D}}_{\alpha}(\mathbf{k})\sin^2\frac{\varphi_{\mathbf{k}}}{2} \approx J^{DD}_{\alpha}(\mathbf{k})\cos\varphi_{\mathbf{k}},$$

$$J^{AS}_{\alpha}(\mathbf{k}) = [J^{DD}_{\alpha}(\mathbf{k}) - J^{\underline{D}\,\underline{D}}_{\alpha}(\mathbf{k})]\sin\frac{\varphi_{\mathbf{k}}}{2}\cos\frac{\varphi_{\mathbf{k}}}{2} \approx J^{DD}_{\alpha}(\mathbf{k})\sin\varphi_{\mathbf{k}}. \quad \text{(B4)}$$

Again, the labels $\underline{D}$ and $\mathbf{k}$ refer to the $\mathbf{k}\pm\mathbf{Q}$ states in the D band of the model A, and $\gamma^{AA}_{\alpha\alpha}(\mathbf{k};2) \approx \gamma^{DD}_{\alpha\alpha}(\mathbf{k})\cos\varphi_{\mathbf{k}}$ in Eq. (4).

[1] C.M. Varma, Int. J. Mod. Phys. B 3 (1989) 2083.
[2] J. Ruvalds, A. Virosztek, Phys. Rev. B 43 (1991) 5498; A. Virosztek, J. Ruvalds, Phys. Rev. B 45 (1992) 347.
[3] M. Opel, R. Nemetschek, C. Hoffmann, R. Philipp, P.F. Müller, R. Hackl, I. Tütto, A. Erb, B. Revaz, E. Walker, H. Berger, L. Forró, Phys. Rev. B 61 (2000) 9752.
[4] S. Uchida, T. Ido, H. Takagi, T. Arima, Y. Tokura, S. Tajima, Phys. Rev. B 43 (1991) 7942.
[5] S.L. Cooper, D. Reznik, A. Kotz, M.A. Karlow, R. Liu, M.V. Klein, W.C. Lee, J. Giapintzakis, D.M. Ginsberg, B.W. Veal, A.P. Paulikas, Phys. Rev. B 47 (1993) 8233.
[6] M.A. Quijada, D.B. Tanner, F.C. Chou, D.C. Johnston, S.-W. Cheong, Phys. Rev. B 52 (1995) 15 485.
[7] S. Lupi, P. Calvani, M. Capizzi, P. Roy, Phys. Rev. B 62 (2000) 12 418.
[8] F. Venturini, Q.-M. Zhang, R. Hackl, A. Lucarelli, S. Lupi, M. Ortolani, P. Calvani, N. Kikugawa, T. Fujita, Phys. Rev. B 66 (2002) 060502.
[9] S. Sugai, S.I. Shamoto, M. Sato, Phys. Rev. B 38 (1988) 6436; S. Sugai, N. Hayamizu J. Phys. Chem. Solids 62 (2001) 177; S. Sugai, T. Hosokawa, Phys. Rev. Lett. 85 (2000) 1112.
[10] J.G. Naeini, X.K. Chen, J.C. Irwin, M. Okuya, T. Kimura, K. Kishio, Phys. Rev. B 59 (1999) 9642.
[11] M.J. Rozenberg, G. Kotliar, H. Kajueter, G.A. Thomas, D.H. Rapkine, J.M. Honig, P. Metcalf, Phys. Rev. Lett. 75 (1995) 105.
[12] E. Dagotto, A. Moreo, F. Ortolani, J. Riera, D.J. Scalapino, Phys. Rev. B 45 (1992) 10 107; J.A. Riera, E. Dagotto, Phys. Rev. B 50 (1994) 452.
[13] J. Jaklič, P. Prelovšek, Phys. Rev. B 50 (1994) 7129.
[14] P. Prelovšek, A. Ramšak, I. Sega, Phys. Rev. Lett. 81 (1998) 3745.
[15] D.N. Basov, E.J. Singley, S.V. Dordevic, Phys. Rev. B 65 (2002) 054516.
[16] F. Marsiglio, J.P. Carbotte, E. Schachinger, Phys. Rev. B 65 (2001) 014515.
[17] E.Ya. Sherman, C. Ambrosch-Draxl, Solid State Commun. 115 (2000) 669; E.Ya. Sherman, C. Ambrosch-Draxl, O. V. Misochko, Phys. Rev. B 65 (2002) 140510.
[18] I. Kupčić, S. Barišić, unpublished.
[19] V.J. Emery, S.A. Kivelson, Phys. Rev. Lett. 71 (1993) 3701.
[20] V.J. Emery, Phys. Rev. Lett. 58 (1987) 2794.
[21] I. Kupčić, unpublished.
[22] A. Schwartz, M. Dressel, G. Grüner, V. Vescoli, L. Degiorgi, T. Giamarchi, Phys. Rev. B 58 (1998) 1261; V. Vescoli, L. Degiorgi, M. Dressel, A. Schwartz, W. Henderson, B. Alavi, G. Grüner, J. Brinckmann, A Virosztek, Phys. Rev. B 60 (1999) 8019.
[23] V. Vescoli, L. Degiorgi, W. Henderson, G. Grüner, K.P. Starkey, L. K. Montgomery, Science 281 (1998) 1181.
[24] T. Giamarchi, Physica B 230-232 (1997) 975; Phys. Rev. B 44 (1991) 2905.
[25] I. Kupčić, Physica B 322 (2002) 154.
[26] G. Kotliar, P.A. Lee, N. Read, Physica C 153-155 (1988) 538; G. Kotliar, in: V.J. Emery (Ed.), Correlated Electron Systems, World Scientific, Singapore, 1992, p. 118.
[27] M. Grilli, B.G. Kotliar, A.J. Millis, Phys. Rev. B 42 (1990) 329.
[28] H. Nikšić, E. Tutiš, S. Barišić, Physica C 241 (1995) 247.
[29] I. Kupčić, Phys. Rev. B 61 (2000) 6994.
[30] E.Ya. Sherman, C. Ambrosch-Draxl, Phys. Rev. B 62 (2000) 9713.
[31] I. Mrkonjić, S. Barišić, cond-mat/0103057.
[32] S. Uchida, H. Takagi, Physica C 162-164 (1989) 1677.
[33] H. Ding, T. Yokoya, J.C. Campuzano, T. Takahashi, M. Randeria, M.R. Norman, T. Mochiku, K. Kadowaki, J. Giapintzakis, Nature 382 (1996) 51.
[34] A. Lanzara, P.V. Bogdanov, X.J. Zhou, S.A. Kellar, D.L. Feng, E.D. Lu, T. Yoshida, H. Eisaki, A. Fujimori, K. Kishio, J.-I. Shimoyama, T. Noda, S. Uchida, Z. Hussain, Z.-X. Shen, Nature 412 (2001) 510.
[35] P.D. Johnson, T. Valla, A.V. Fedorov, Z. Yusof, B.O. Wells, Q. Li, A.R. Moodenbaugh, G.D. Gu, N. Koshizuka, C. Kendziora, Sha Jian, D.G. Hinks, Phys. Rev. Lett. 87 (2001) 177007.
[36] T. Yoshida, X.J. Zhou, M. Nakamura, S.A. Kellar, P.V. Bogdanov, E.D. Lu, A. Lanzara, Z. Hussain, A. Ino, T. Mizokawa, A. Fujimori, H. Eisaki, C. Kim, Z.-X. Shen, T. Kakeshita, S. Uchida, Phys. Rev. B 63 (2001) 220501.
[37] R. Liu, B.W. Veal, A.P. Paulikas, J.W. Downey, P.J. Kostić, S. Fleshler, U. Welp, C.G. Olson, X. Wu, A.J. Arko, J.J. Joyce, Phys. Rev. B 46 (1992) 11 056.
[38] A. Ino, C. Kim, T. Mizokawa, Z.-X. Shen, A. Fujimori, M. Takaba, K. Tamasaku, H. Eisaki, S. Uchida, J. Phys. Soc. Jpn. 68 (1999) 1496.
[39] K. Ishida, Y. Kitaoka, G.-Q. Zheng, K. Asayama, J. Phys. Soc. Jpn. 60 (1991) 3516.
[40] S. Ohsugi, Y. Kitaoka, K. Ishida, G.-Q. Zheng, K. Asayama, J. Phys. Soc. Jpn. 63 (1994) 700.
[41] I. Kupčić, S. Barišić, E. Tutiš, Phys. Rev. B 57 (1998)

8590.
[42] D. Pines, P. Noziéres, The Theory of Quantum Liquids I, Addison-Wesley, New York, 1989, Chapter 4.
[43] P.W. Anderson, The Theory of Superconductivity in the High-T_c Cuprates, Princeton University Press, Princeton, 1997 and references therein.
[44] D.B. Tanner, F. Gao, K. Kamarás, H.L. Liu, M.A. Quijada, D.B. Romero, Y-D. Yoon, A. Zibold, H. Berger, G. Margaritondo, L. Forró, R.J. Kelly, M. Onellion, G. Cao, J.E. Crow, Beom-Hoan O, J.T. Markert, J.P. Rice, D.M. Ginsberg, Th. Wolf, Physica C 341-348 (2000) 2193.
[45] J. Friedel, M. Kohmoto, Eur. Phys. J. B 30 (2002) 427.
[46] J.W. Loram, K.A. Mirza, J.R. Cooper, J.T. Tallon, J. Phys. Chem. Solids 59 (1998) 2091.
[47] E. Tutiš, Ph. D. thesis, University of Zagreb, 1994.
[48] A.A. Abrikosov, V.M. Genkin, Zh. Eksp. Teor. Fiz. 65 (1973) 842 (Sov. Phys. JETP 38 (1974) 417).
[49] T.P. Devereaux, Phys. Rev. B 45 (1992) 12 965.